Flow Measurement and Instrumentation 43 (2015) 34–46

Contents lists available at ScienceDirect

Flow Measurement and Instrumentation

journal homepage: www.elsevier.com/locate/flowmeasinst

Determining the discharge rate from a submerged oil leak jet using ROV video

Frank Shaffer [a,*], Ömer Savaş [b], Kenneth Lee [b], Giorgio de Vera [b]

[a] USDOE National Energy Technology Laboratory, United States
[b] U.C. Berkeley, Department of Mechanical Engineering, United States

ARTICLE INFO

Article history:
Received 4 February 2014
Received in revised form
15 December 2014
Accepted 27 December 2014
Available online 9 January 2015

Keywords:
Flow rate
Leak rate
Oil leak
Particle Image Velocimetry (PIV)
Deepwater horizon

ABSTRACT

With expanded deep sea drilling in the Gulf of Mexico, and possibly the Arctic, it is imperative to have a technology available to quickly and accurately measure the discharge rate from a submerged oil leak jet. This paper describes an approach to measure the discharge rate using video from a Remotely Operated Vehicle (ROV). ROV video can be used to measure the velocity of visible features (turbulent eddies, vortices, entrained particles) on the boundary of an oil leak jet, from which the discharge rate can be estimated. This approach was first developed by the Flow Rate Technical Group (FRTG) Plume Team, of which the authors Savaş and Shaffer were members, during the response to the Deepwater Horizon (DWH) oil leak. Manual tracking of visible features produced the first accurate government estimates of the oil discharge rate from the DWH. However, for this approach to be practical as a routine response tool, software is required that automatically measures the velocity of visible features. To further develop this approach, experiments were conducted to simulate a submerged oil leak jet using a dye-colored water jet in the U.C. Berkeley Tow Tank facility. Jet exit diameters were 10.2 cm and 20.3 cm. With flow rates up to 11 gal/s, Reynolds numbers in the range of the DWH oil leak jets (up to 500,000) were achieved. The dye-colored water jets were recorded with high speed video and radial profiles of velocity were mapped with Laser Doppler Anemometry (LDA). Particle Image Velocimetry (PIV) software was applied to measure the velocity of visible features. The velocities measured with PIV software were in good agreement with the LDA measurements. Finally, the PIV software was applied to ROV video of the DWH oil leak jet. The measured velocities were 10–50% lower than manual measurements of velocity. More research is required to determine the reasons why PIV software produced much lower velocities than manual tracking for the DWH oil leak jet.

Published by Elsevier Ltd.

1. Introduction

On April 21, 2010, the Deepwater Horizon (DWH) failed catastrophically and produced oil leaks in the form of submerged turbulent jets located 1500 m below the sea surface. To determine the type and level of response required, an accurate estimate of the oil leak rate was needed. However, at that time, a proven technology to measure the leak rate from a deep sea oil leak jet was not available. The National Commission on the DWH Oil Spill [18] concluded the oil leak rate was grossly underestimated during the first two months and that the underestimates resulted in an inadequate response and caused attempts to cap the well to fail. As the use of deep sea drilling expands and the depths increase, it is of paramount importance to develop an approach to quickly and accurately measure the leak rate from a deep sea oil or gas leak.

During the DWH oil leak, in mid May of 2010, the Flow Rate Technical Group (FRTG) was formed and charged with generating official government estimates of the oil leak rate. The Plume Team of the FRTG was given ROV video of the oil leak jets and asked to quickly produce estimates of the leak rate. The basic approach developed by the Plume Team was to measure the velocity of visible features (turbulent eddies, vortices, particles of hydrates and waxes), then use the boundary velocity to predict the mean velocity over the cross section of the opaque oil jets. Fig. 1 shows consecutive video frames with large visible features propagating at the boundary of the DWH oil leak jet. Due to the low frame rate of 25 per second, only large features persist over the frame interval time. Smaller features with faster deformation rates do not persist over the frame interval time. With the mean velocity, and with assumptions for the amount of entrained water, amount of gas dissolved in the oil, and the jet diameter, an estimate of the total leak rate could be calculated. Before continuing this discussion of this approach to measuring an oil/gas leak rate from a submerged leak jet, a brief description of classical submerged turbulent jets is necessary.

* Corresponding author.

http://dx.doi.org/10.1016/j.flowmeasinst.2014.12.006
0955-5986/Published by Elsevier Ltd.

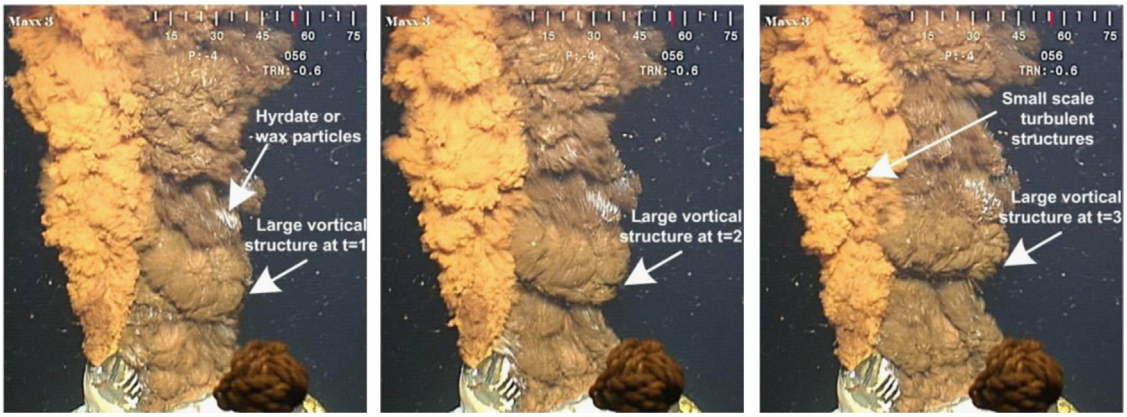

Fig. 1. Consecutive video frames showing examples of visible features propagating in the flow direction on the Deepwater Horizon oil leak jet. The jet diameter was approximately 50 cm and the video frame rate was 25 per second.

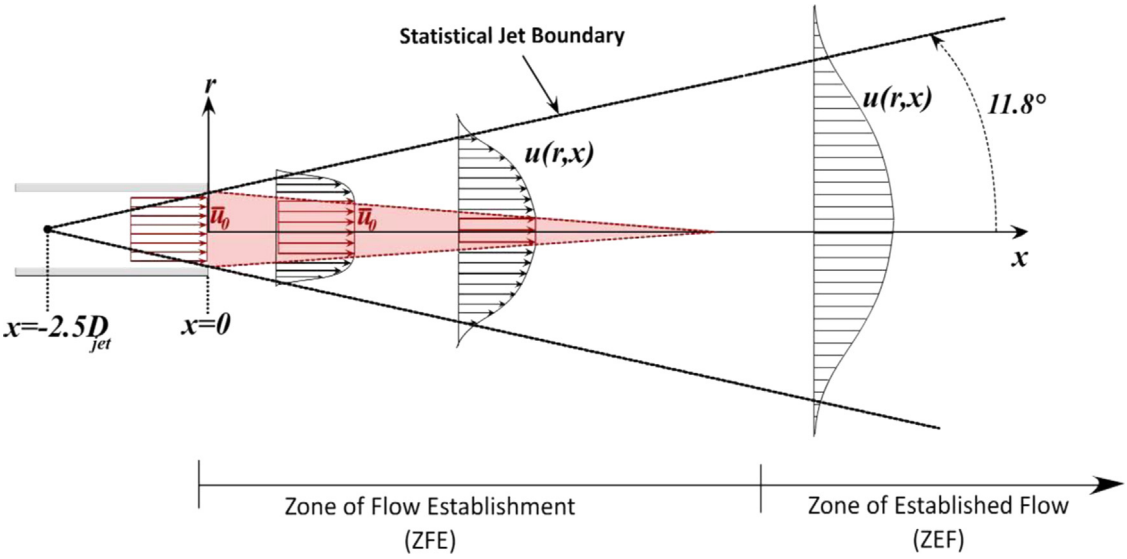

Fig. 2. Velocity profiles and regions of a submerged turbulent jet.

1.1. Submerged turbulent jets

The theory of submerged turbulent jets, both from an Eulerian and Langrangian approach, is well established. Prandtl [20–22] and others developed the theoretical foundation in the 1910s and 1920s. Abramovich [1–4] and others made advances in both experiments and theory between 1930 and 1950. With recent advances in computational fluid dynamics (CFD), the time-averaged behavior of submerged turbulent jets can be accurately simulated, assuming the properties of the jet fluid are known [11,12,27].

Fig. 2 illustrates the zones and velocity profiles of a turbulent pipe flow emitting into an infinite body of fluid at rest. Because the mean streamwise velocity (velocity in the x-direction of the jet centerline) of a submerged turbulent jet is orders of magnitude higher than the mean radial velocity (velocity in the r-direction orthogonal to the jet centerline), the radial velocity can be ignored in many practical applications, except when entrainment is central to the discussion, and will be ignored in this study. For the remainder of this paper, "velocity" will be defined as streamwise velocity.

The centerline velocity at the pipe exit is u_0. For purposes of this discussion, since the radial profile of velocity in a fully developed turbulent pipe flow is nearly flat (of uniform velocity), the radial profile of velocity at the jet exit is assumed to be flat with a value of $\overline{u}_0$ [24], where the overbar denotes average values.

When a submerged axisymmetric turbulent jet discharges into an infinite body of fluid at rest, the edges of the jet shear against the surrounding fluid causing the formation of a mixing layer. The dynamics of the shear layer causes the entrainment of the surrounding fluid into the jet, which causes the jet to expand. The radial profile of streamwise velocity begins as flat at the jet exit, then the shearing action causes the radial profile to transform into a nearly Gaussian profile. All submerged turbulent jets have a divergence angle around 24° (half angle of 12°), depending on how the statistical boundary is defined [13]. The statistical jet boundary is a point on the radial profile of mean streamwise velocity where the value decreases below a predefined level. Albertson [2], Miller and Comings [17] and Bradbury [3] define the statistical boundary velocity as equal to $1/e$ of the centerline. The statistical jet boundary lines converge at a focal point at a distance of $2.5D_{jet}$ upstream of the jet exit, commonly referred to as the virtual origin.

It is important to note that the velocity at the statistical boundary, u_{sb}, is not the same as the mean velocity of visible features, u_{vf}, i.e., $u_{vf} \neq u_{sb}$.

The distance from the jet exit in which the jet has a constant velocity core of $\overline{u}_0$ (the diverging area shaded in red) is called the Zone of Flow Establishment (ZFE). For a submerged jet exiting from a round exit, the ZFE is 6.2 exit diameters ($6.2D_{jet}$) long [13]. The boundaries of the constant velocity core (called the potential core when the discharge flow profile is irrotational) are formed by points where the velocity decreases infinitesimally below $\overline{u}_0$.

Downstream of the ZFE is the Established Flow Zone (EFZ). In the EFZ, radial profiles of mean streamwise velocity are Gaussian

and self-similar. Self-similar means that at any distance, x, all data for mean velocity fall onto the same radial profile when plotted in the non-dimensional form of $u(r)/u_c$ and r/R_{jet}, where u_c is the centerline velocity at x and R_{jet} is the radius of the jet at x.

Lee and Chu [13] derive equations for the radial profiles of velocity and concentration in a submerged turbulent jet. In the ZFE, inside the constant velocity core, for $r < R_{core}(x)$, where $R_{core}(x)$ is the half width of the constant velocity core, the velocity and concentration (fraction of fluid at any point that is jet fluid) are given by

$$u(x,r) = u_0, \quad c(x,r) = c_0 \tag{1}$$

In the ZFE, outside of the constant velocity core, where $r > R_{core}$, the velocity and concentration are given by

$$u = u_0 \exp\left[-\frac{(r-R_{core}(x))^2}{b(x)^2}\right], \quad c = c_0 \exp\left[-\frac{(r-R_{core}(x))^2}{\lambda^2 b(x)^2}\right] \tag{2}$$

where b is the half width of the jet from the centerline to the statistical jet boundary and λ is a turbulent diffusion coefficient. In the EFZ, the velocity profile is given by

$$u = u(x,0) \exp\left[-\frac{r^2}{b(x)^2}\right], \quad c = c(x,0) \exp\left[-\frac{r^2}{\lambda^2 b(x)^2}\right] \tag{3}$$

The half width of the jet is given by $b = \beta x$, where β is the slope of the statistical jet boundary. The experimental work of Albertson [2] and Wygnanski and Fiedler [31] found that $\beta = 0.114$ for a submerged turbulent jet emitting from a round orifice. The diffusion coefficient, λ, is equal to the ratio of the divergence angle of the statistical concentration boundary to the divergence angle of the statistical jet boundary. Experimental work of Papanicolaou and List [19] found that $\lambda = 1.2$ for a submerged turbulent jet, indicating that the concentration half width is larger than the velocity half width.

1.2. Measurement of the flow/leak rate from a submerged turbulent jet

The following expression was used by members of the Plume Team in 2010 to calculate oil leak rates:

$$\dot{Q}_{oil} = \overline{u}(x) A_{jet}(x)[1 - X_{GOR}]E(x) \tag{4}$$

where $\overline{u}(x)$ is the average jet velocity at a downstream distance, x, from the jet exit, $A_{jet}(x)$ is the cross sectional area of the jet at a distance downstream from the jet exit, X_{GOR} is the volume fraction of methane gas dissolved in the oil. Near the jet exit, methane was dissolved in the oil. Downstream the methane was liberated from the oil and $E(x)$ is the ratio of the volume of oil minus sea water entrained into the jet to the total jet volume at any distance x.

The jet cross sectional area, $A_{jet}(x)$, can be found by measuring the jet diameter from the ROV video at the distance x where visible jet boundary velocity was measured. The gas-to-oil ratio, X_{GOR}, was found by sampling the oil with ROV probes and bringing it to the surface for analysis [25]. The gas-to-oil ratio was assumed to be constant. The entrainment parameter, $E(x)$, can be found by measuring the expansion of the jet, or by using theory such as that of Lee and Chu [13] as described above in Eqs. (1)–(3).

Several challenges were encountered in applying this approach. The first challenge was how to measure the velocity of visible features on the boundary of the immiscible oil leak jets. Six members of the Plume Team began by using Particle Image Velocimetry (PIV) software to automatically measure the velocity of visible features. Three of the members (Leifer, Savaş and Shaffer) who began using PIV software concluded that it was producing erroneously low values of velocity [10]. They resorted to manual tracking of larger, faster visible features by hand. It was later determined that PIV software led to erroneously low estimates of the oil leak rate [16,23].

The next challenge was to determine the relationship between the velocity of visible features, u_{vf}, and the mean velocity of the jet, $\overline{u}(x)$. During the work of the Plume Team and during this study,

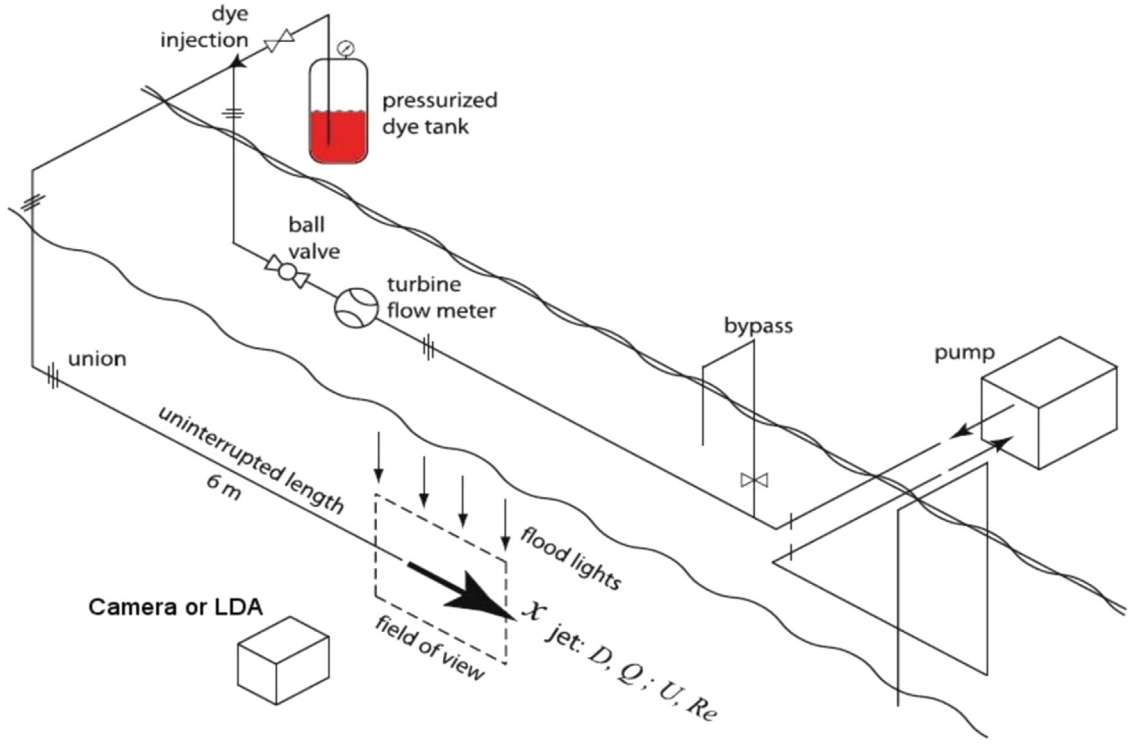

Fig. 3. Experimental setup for flow visualization at Berkeley Tow Tank.

literature searches found no experimental data to relate u_{vf} to $\overline{u}(x)$. Therefore, each member of the Plume Team had to make an educated guess for the relationship between u_{vf} and $\overline{u}(x)$. It is important to note that u_{vf} is not the same as the velocity at the statistical jet boundary, u_{sb}. The statistical jet boundary velocity, u_{sb}, is a statistical point on the radial profile of mean jet velocity, $\overline{u}_{jet}$.

The final challenge was to estimate the amount of water entrained into the oil jet, $E(x)$. The amount of entrainment can be calculated using the expansion of the jet, however, because the instantaneous boundary is constantly changing, an accurate measurement of the time-averaged jet expansion can be difficult.

The Plume Team overcame the challenges of the radial velocity profile and entrainment by making measurements of the velocity of visible features close to the jet exit, within, $x/D < 2$, in the ZFE. An assumption was made that coherent structures this close to the jet exit are sampling the constant velocity core, and therefore moving at the velocity of the core. Because entrainment is negligible at $x/D < 2$, and because the cross sectional area of the jet exit was used, the need for an estimate of entrainment was eliminated.

2. Description of UC Berkeley tow tank experiments

The authors of this paper have continued to develop this ROV video based approach since the DWH crisis. In October of 2010, Savaş [23] conducted experiments to simulate a large, submerged oil leak using a submerged, 10.1 cm diameter, dye-colored water jet in the U.C. Berkeley Tow Tank facility. The Tow Tank is 1.8 m deep, 2.4 m wide, and 67 m long. Submerged turbulent jets of dye-colored water were created at the midpoint of the Tow Tank, thereby avoiding wall effects. As will be explained later, LDA measurements confirmed that recirculation caused by wall effects were negligible.

The flow circuit used to create the submerged turbulent jet is shown in Fig. 3. Water is supplied to the submerged jet though Schedule 40, white PCV pipe of 10.1 cm inner diameter (4 in.) and a total length of approximately 20 m. Water is drawn from the tow tank through 10.1 cm diameter PVC pipe with a length of about 5 m. Before the jet exit, a straight, uninterrupted length of about 6.1 m ($L/D=60$) allows for a fully developed turbulent pipe flow at the jet exit [14,15]. The internal surfaces of the pipes have a measured relative roughness of about 0.001. The effect of the roughness was not considered in this study.

For Savaş's experiments in late 2010, water flow was supplied to the jet with a 9 HP gasoline centrifugal impeller pump (Duromax – XP904WP – 427 GPM). The impeller has three vanes and was run at 60 revolutions per sec (RPS). Thus, it can be expected that the pump will produce slight pressure/flow variations in the range of 180 Hz. To damp pressure fluctuations from the impeller pump, the pump is connected to the PVC pipe with 2.2 m length sections of flexible tubing on both the suction and discharge sides. As will be explained later, a frequency analysis of LDA data taken at the jet exit did not show dominant frequencies in the ranges expected from the pump impellers, indicating that the pump frequencies had been damped by the jet exit. The flexible tubing connecting the pump, the flow control valves, the turbine meter and 20 m of PVC pipe between the pump and the jet exit was sufficient to damp flow fluctuations caused by the pump.

The Duromax pump supplied flow rates of up to 4.8 gal/s to produce Reynolds numbers up to 220,000 with the 10.1 cm diameter jet exit. The Reynolds numbers of the DWH oil leak were in the range of 5×10^5–10^6. The flow rate was measured with a turbine flow meter (GPI Model TM400N) with a listed accuracy of $\pm 2\%$. The dye-colored jet was recorded with a high definition video camera with pixel resolution of 1920×1080 and a frame rate of 60 per second. The exposure time was set at 10 ms.

Fig. 4. Flow visualization with dye point injection. Water flow rate was 41.7 l/s (11 gal/s) producing a Reynolds number of 500,000. The camera frame rate was 1500/s and the exposure time was 0.75 ms.

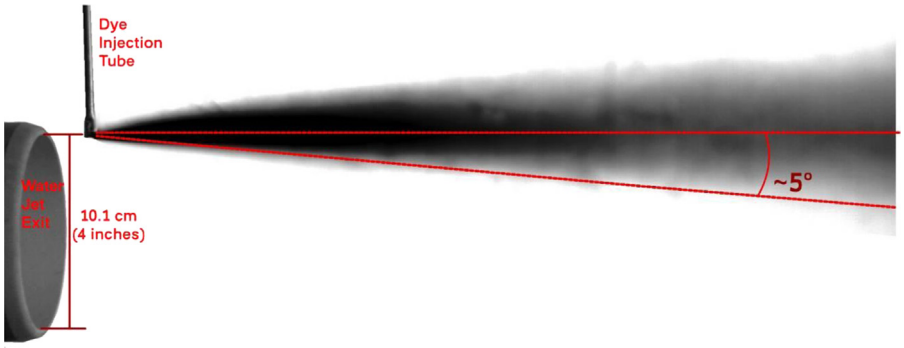

Fig. 5. Gray levels averaged over 2000 video frames with dye injector at $r/R=0.95$ and $x/D=0.20$.

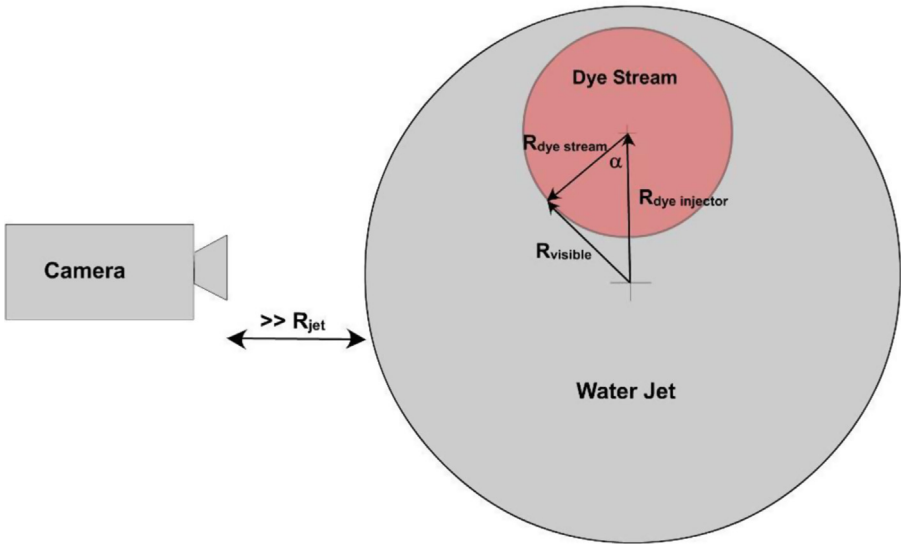

Fig. 6. Slice through the water jet tangential to jet centerline illustrating the expansion of dye stream.

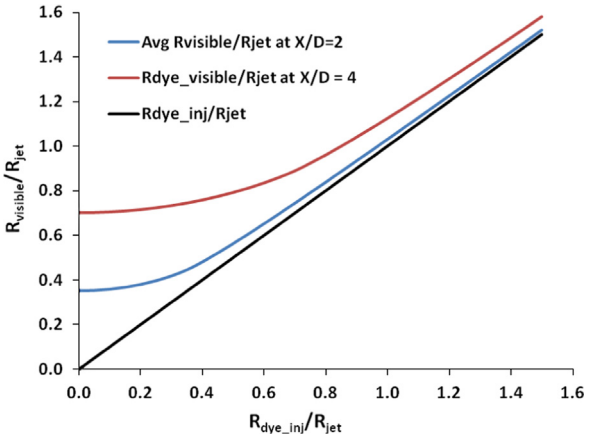

Fig. 7. Comparison of the average $R_{visible}$ and $R_{dye\_injection}$ at downstream distances of $x/D=2$ and 4.

In July of 2012, the authors of this paper conducted additional testing in the Berkeley Tow Tank with higher flow rates and better instrumentation. A diesel centrifugal pump (Power Prime Pumps, Model DV-100) was used to create flow rates up to 41.7 l/s (11 gal/s), thereby producing Reynolds numbers up to 5×10^5, within the range of the DWH oil leak jets. The DV-100 pump has a three-vane impeller that runs at 1400–2200 rpm. Thus, slight pressure/flow fluctuations with frequencies in the range of 70–110 Hz would be expected from the pump. A frequency analysis of LDA data at the jet exit did not show dominant frequencies at 70–110 Hz or harmonics of these frequencies, indicating that fluctuations from the impeller pump were damped by the jet exit.

The water jets were emitting from either a 10.1 cm diameter pipe or a 10.1 cm orifice at the end of a 20.2 cm diameter pipe. The edges of the orifice were smoothed and rounded.

The dye-colored jets were recorded with a high definition, high speed video camera (Vision Research Model v341) at frame rates up to 1500 per second at resolutions up to 2560 × 1100 pixels. The exposure time was 1.0 ms or less. Thus, frame rates were an order of magnitude higher and exposure times an order of magnitude lower than the October 2010 experiments [23]. This provided better temporal resolution of the rapidly changing flow features.

Two types of dye coloring of the water jet were used. The entire jet was dyed or "point" injection of dye was used. With point injection, dye is injected at a low velocity through a tube with an inner diameter of 3.175 mm (1/8 in.). To reduce flow disturbance, the end of the tube was tapered in the form of an air foil with the longest dimension aligned with the jet. Visual observations indicated minimal turbulence or vortex shedding caused by the dye injector. Fig. 4 shows point injection of dye in a water jet with a 4 in. diameter exit.

Turbulent diffusion caused the dye stream to expand radially. Fig. 5 shows the average gray level of the dye stream over 2000 video frames with the injector at the same position. The half angle of the dye expansion is about 5°.

Because of the expansion of the dye stream, the camera is viewing the outer boundary of the dye stream. Fig. 6 illustrates a slice through the jet tangential to the centerline. As will be explained below, PIV software was applied to the high speed video to measure the velocity of dyed flow features. Since the camera is viewing the outer boundary of the dye stream, the actual radial position of dyed features seen by the camera is at, $R_{visible}$, which is not the same as the radial position of the dye injector, $R_{dye\_injector}$.

To account for the effect of the expanding dye stream, an average radial position of the dye seen by the camera, $\overline{R}_{visible}$ was calculated. Using the Law of Cosines, $R_{visible}$, is calculated at points along the perimeter of the dye stream from $\alpha=0°$ to 180°, where $\alpha=0°$ is pointing vertically downward and $\alpha=180°$ is pointing vertically upward, then the values of $R_{visible}$ are averaged as

$$\overline{R}_{visible} = \sqrt{\frac{1}{n_\alpha}\sum_{\alpha=0°}^{\alpha=180°}\left[R_{dye\_inj}^2 + R_{dye\_stream}^2 - 2R_{dye\_inj}R_{dye\_stream}\cos\alpha\right]}$$

Substituting the radius of the dye stream, $R_{dye\_stream} = x \tan(\Phi_{dye\_stream})$, where Φ_{dye_stream} is the divergence half angle of the dye stream, gives

$$\overline{R}_{visible} = \sqrt{\frac{1}{n_\alpha}\sum_{\alpha=0°}^{\alpha=180°}\left[R_{dye\_inj}^2 + (R_{dye\_stream}\tan\Phi_{dye\_stream})^2 - 2R_{dye\_inj}R_{dye\_stream}\tan\Phi_{dye\_stream}\cos\alpha\right]}$$

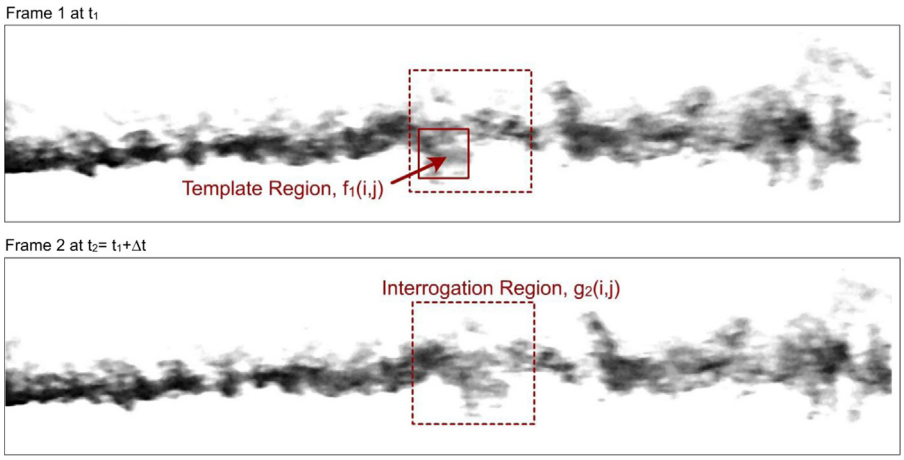

Fig. 8. Illustration of template and interrogation regions in two consecutive video frames.

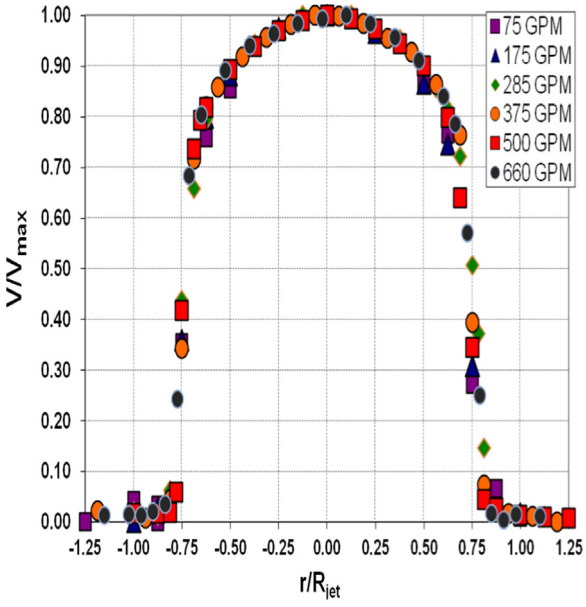

Fig. 9. Radial profiles of mean streamwise velocity measured with LDA for 10.1 cm diameter pipe jet at $x=0.25D$.

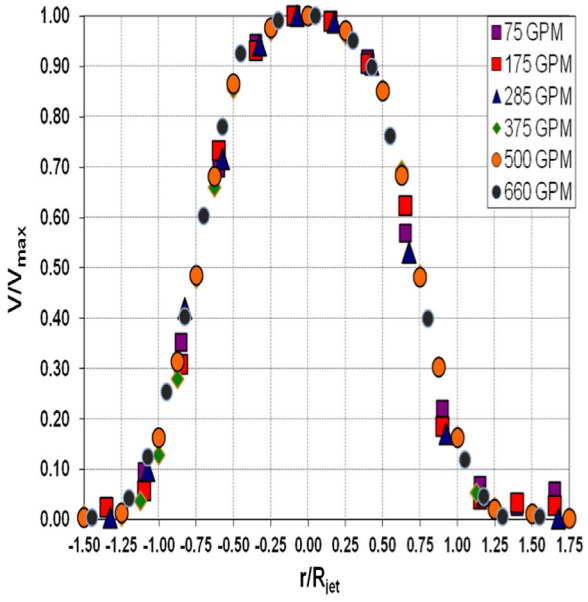

Fig. 10. Radial profiles of mean streamwise velocity measured with LDA for 10.1 cm diameter pipe jet at $x=2.0D$.

Fig. 7 shows the result of the calculation of $\overline{R}_{visible}$ at downstream distances where LDA data was taken, $x/D=2$ and 4. All radial profiles of streamwise velocity as measured with PIV software have the radial position corrected for expansion of the dye stream.

To measure the velocity of dyed flow features, the high speed video was analyzed with a PIV code developed by Tseng [28–30] The code is implemented as a plugin for ImageJ, an image analysis tool developed by the National Institutes of Health (NIH) [26].

The PIV tool by Tseng is based on a template matching approach. Two consecutive video frames are selected and the second frame is divided into interrogation regions as shown in Fig. 8. A smaller "template" region from the first frame is cross-correlated over the interrogation region of the second frame. The template cross-correlation can be described as

$$\Phi_{fg}(m,n)=\sum_{m}\sum_{n}f_1(i+m,j+n)g_2(i,j)$$

where $f_1(i, j)$ is the gray level array of template region in frame 1 and $g_2(i, j)$ is the gray level array of the interrogation region in frame 2. The subscripts m and n are the center position of the template over the interrogation region when a cross-correlation is calculated. The result is a correlation peak that measures the average displacement of the template region from frame 1 to frame 2. The correlation peak measures the average distance a dyed flow feature moved from the first video frame to the second. With the time between video frames, Δt, a velocity vector is calculated for each interrogation region. A threshold for the correlation peak can be set to reject poor correlations.

Large interrogation regions of around 200×200 pixels with a template region of around 100×100 pixels gave the best results, i.e., the best match with LDA data below. This is likely because larger flow features, with dimensions around 100×100 pixels for these experiments, tended to persist longer than smaller flow features. Additional research is being conducted to determine how to choose optimal sizes for interrogation regions [9].

At this point, it should be noted that the measurements being performed with PIV software are not traditional PIV measurements. PIV is actually a type of "Image Correlation Velocimetry (ICV)." ICV uses cross correlation of regions in consecutive video frames to measure the displacements of moving images. With PIV, the images are of seed particles which have been added to a transparent flow field that is being illuminated by a sheet of laser light. For this application, there are no seed particles in the flow field and it is not illuminated with a sheet of laser light. The images are of visible features at the

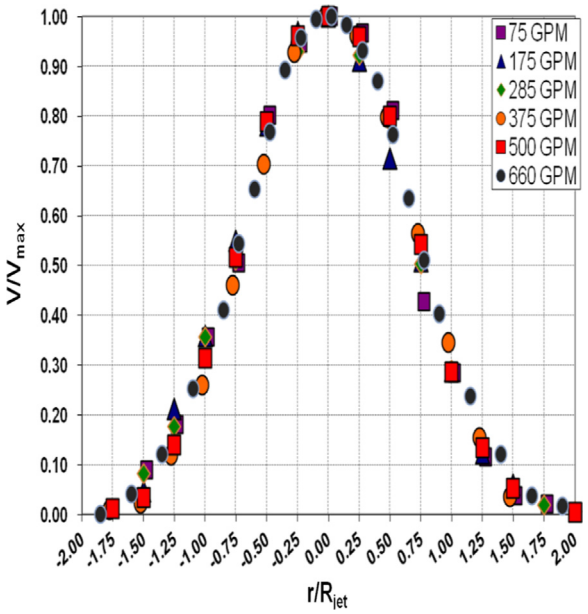

Fig. 11. Radial profiles of mean streamwise velocity measured with LDA for 10.1 cm diameter pipe jet at $x=4.0D$.

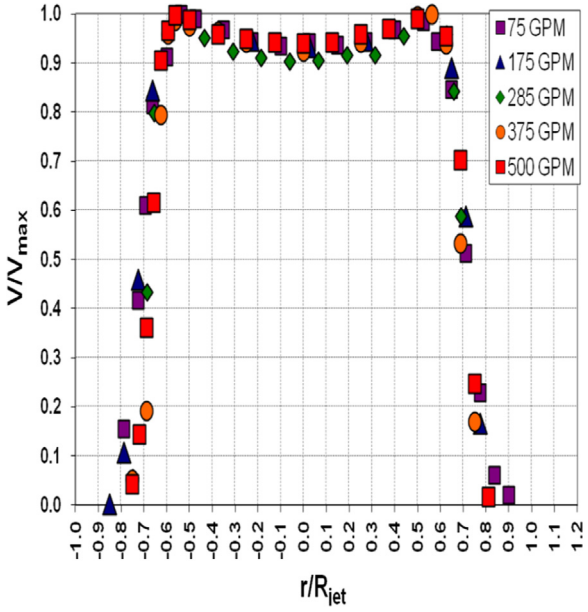

Fig. 12. Radial profiles of mean streamwise velocity measured with LDA for 10.1 cm diameter orifice at $x=0.25D$.

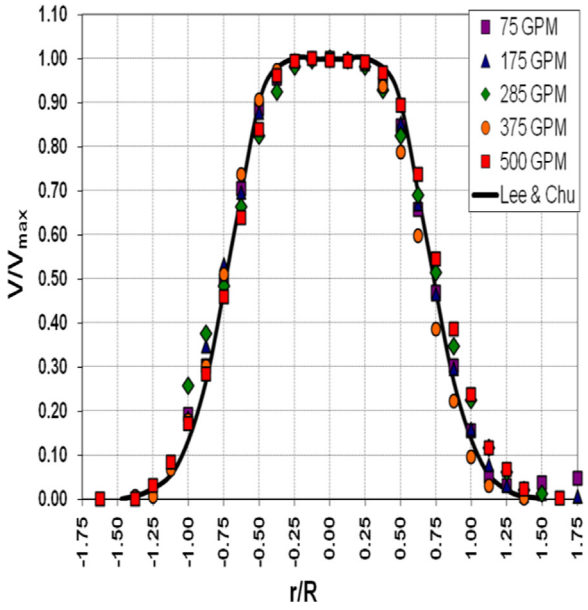

Fig. 13. Radial profiles of mean streamwise velocity measured with LDA for 10.1 cm diameter orifice at $x=2.0D$.

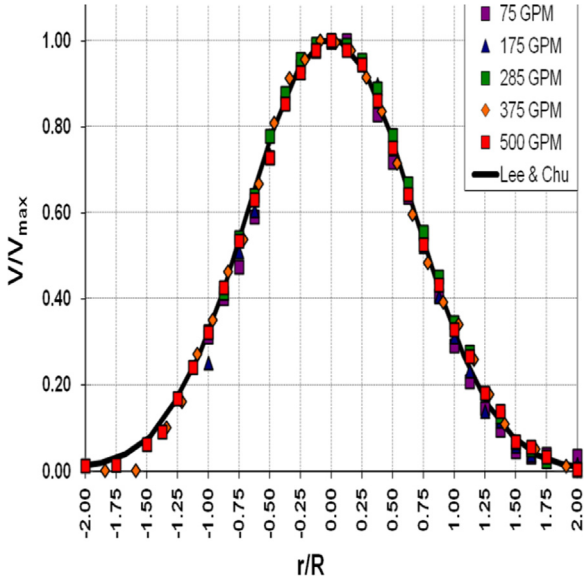

Fig. 14. Radial profiles of mean streamwise velocity measured with LDA for 10.1 cm diameter orifice at $x=4.0D$.

boundary of a submerged jet. This application is more appropriately called Image Correlation Velocimetry (ICV). For the remainder of this paper, the term ICV will be used. However, it should be understood that ICV means the application of software developed for PIV to measure the velocity of visible features at the boundary of a submerged jet.

Before the ICV analysis was performed, the high speed video was enhanced. To remove low frequency variations in gray levels caused by non-uniform illumination, a high pass Fast Fourier Transform (FFT) was performed to remove variations larger than $\frac{1}{4}$ of the maximum dimension of the video frame. The tubing producing the jet and the dye injection tube was removed from the video. The gray levels were inverted and contrast enhancement steps were applied to result in gray levels of zero outside of the dyed flow features. Some of the video was enhanced with an edge detection Sobel filter to increase the signal-to-noise ratio of visible features, but a systematic study of the effect of the Sobel filter was not performed. Choice of optimal enhancement filters is being studied in the ongoing DOI-BSEE project [9].

The radial profiles of streamwise velocity of the jet were also mapped with a Dantec FlowExplorer Laser Doppler Anemometer (LDA) [8] at downstream distances of $x/D_{jet}=0.25$, 2.0 and 4.0. A 300 mm focal length lens was used. The LDA was operated in non-coincidence mode. The jet flow was seeded with 50 μm diameter silver coated ceramic spheres of density 0.8–1.2 g/cm^3.

3. Results

3.1. Laser Doppler anemometry

Figs. 9–14 show LDA measurements of the radial profile of mean streamwise velocity for all flow rates for pipe and orifice

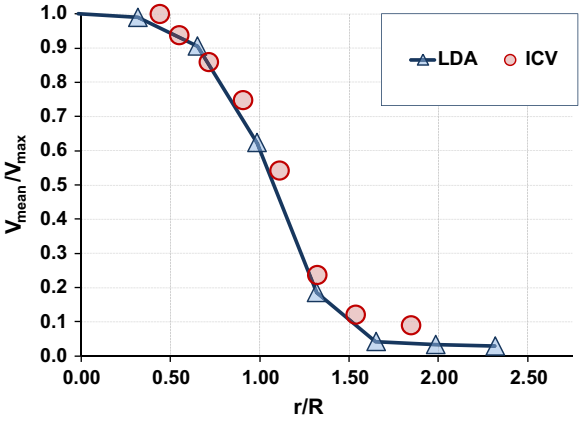

Fig. 15. Radial profiles of streamwise mean velocity at $x/D=2$.

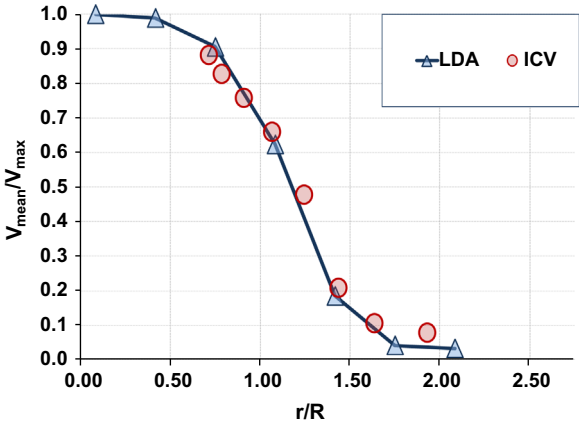

Fig. 16. Radial profiles of streamwise mean velocity at $x/D=4$.

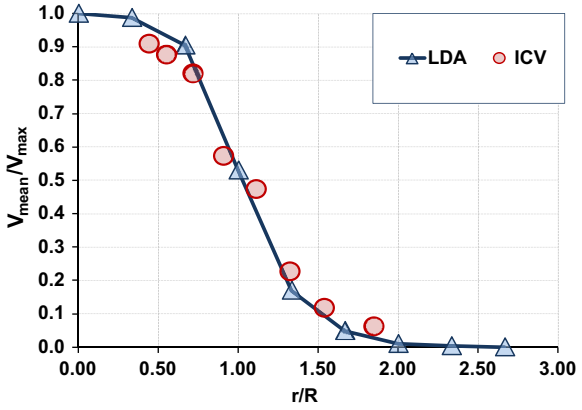

Fig. 17. Radial profiles of streamwise mean velocity at $x/D=2$.

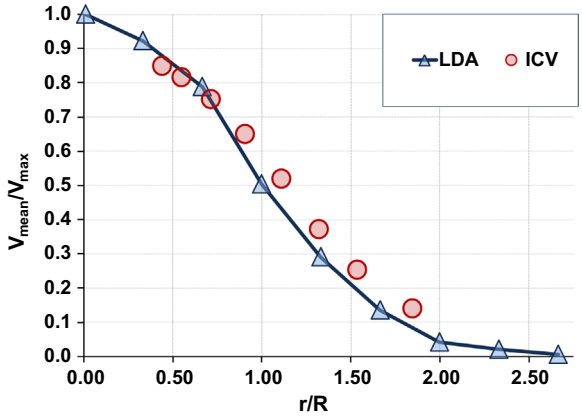

Fig. 18. Radial profiles of streamwise mean velocity at $x/D=4$.

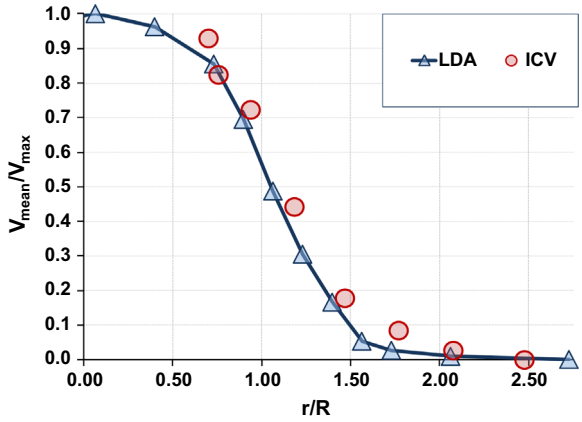

Fig. 19. Radial profiles of streamwise mean velocity at $x/D=2$.

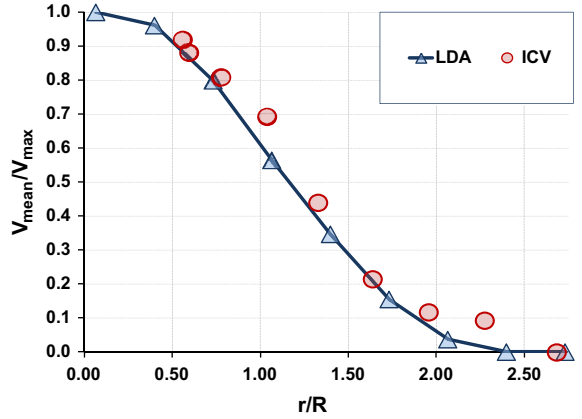

Fig. 20. Radial profiles of streamwise mean velocity at $x/D=4$.

discharges. The plots show mean streamwise velocity normalized with the mean centerline velocity on the ordinate axis and radial distance from the centerline normalized with the jet exit radius on the abscissa axis. Regardless of flow rate, all data fall onto the same profile at each measurement station. LDA measurements were extended outside the jet to ensure that the flow was still outside the jet, indicating negligible wall effects or recirculation currents. The profile for the 10.1 cm diameter orifice shows some "pinching effect" at $x=0.25D$, i.e., the radial profile of velocity shows maxima near the edge of the jet. This was likely caused by the rounded edges of the orifice. The pinching effect dissipates before $x=2.0D$.

Figs. 13 and 14 also show the theoretical predictions from Eqs. (1)–(3) of Lee and Chu. Good agreement with the theory of Lee and Chu further indicates that a classical submerged turbulent jet was created from a fully developed turbulent pipe flow.

3.2. *Image correlation velocimetry of dyed flow features*

Figs. 15–30 show the mean streamwise velocity normalized with the mean centerline velocity and radial distance from the centerline

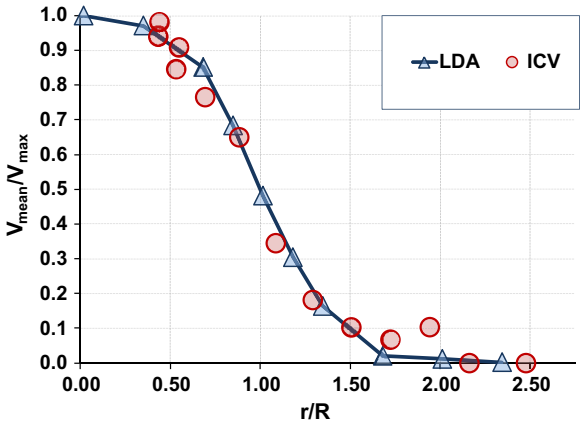

Fig. 21. Radial profiles of streamwise mean velocity at $x/D=2$.

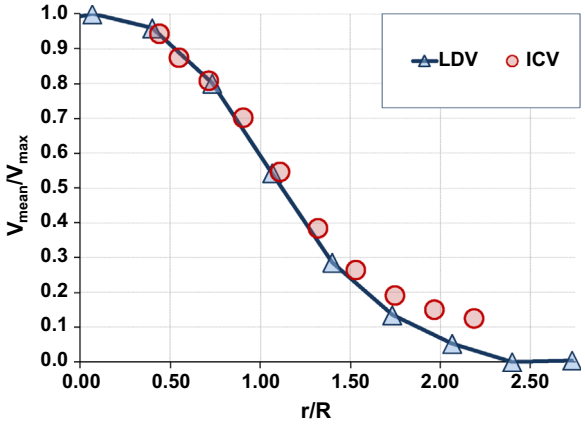

Fig. 22. Radial profiles of streamwise mean velocity at $x/D=4$.

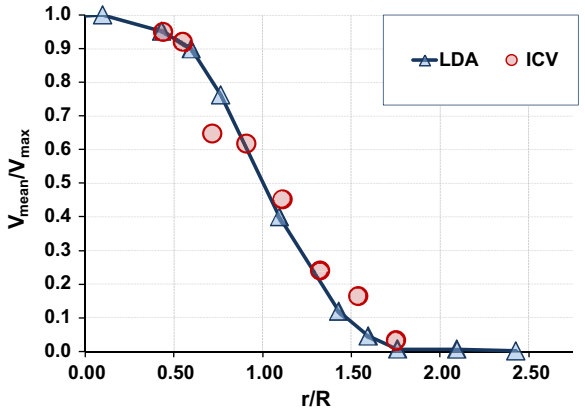

Fig. 23. Radial profiles of streamwise mean velocity at $x/D=2$; 4 in pipe jet; 660 GPM.

normalized with the jet exit radius as measured with ICV. Figs. 15–24 are for pipe discharge and Figs. 25–30 for orifice discharge.

3.2.1. *Pipe jet at 175 GPM (Re=133,000)*

A total of 16,837 video frames were recorded (10,000 video frames were recorded at 700 frames/s and 6837 frames at 1000 frames/s) for a total sample period of 16.6 s. ICV was applied with an interrogation window of 175 × 175 pixels and a subregion template of 125 × 125 pixels. The center of the interrogation region was moved in steps of 50 pixels. The mean velocity at the jet centerline was 1.61 m/s.

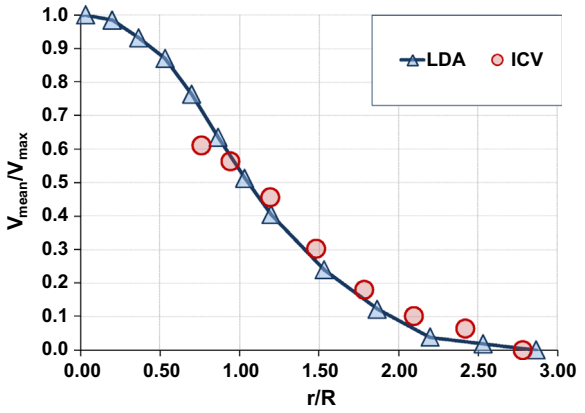

Fig. 24. Radial profiles of streamwise mean velocity at $x/D=4$; 4 in pipe jet; 660 GPM.

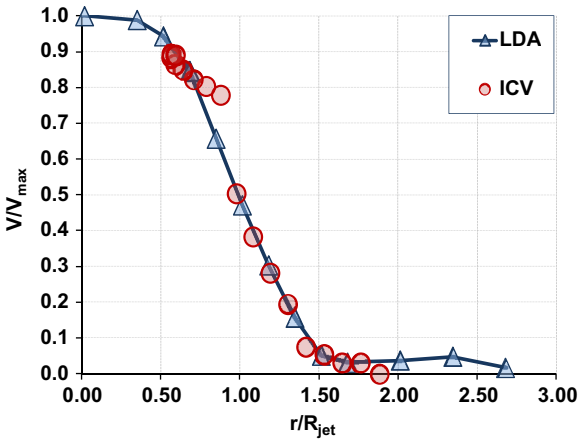

Fig. 25. Radial profiles of streamwise mean velocity at $x/D=2$; 4 in orifice jet; 75 GPM.

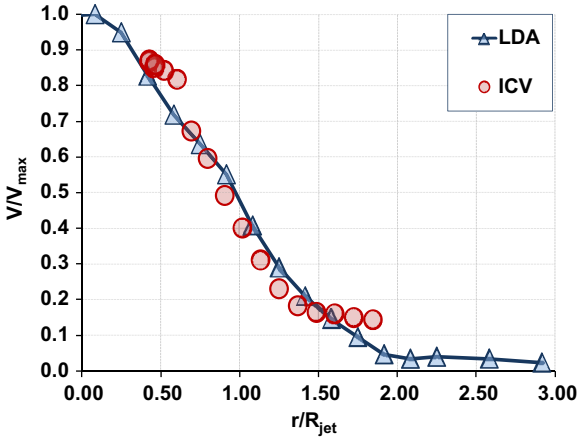

Fig. 26. Radial profiles of streamwise mean velocity at $x/D=4$; 4 in orifice jet; 75 GPM.

3.2.2. *Pipe jet at 285 GPM (Re=217,000)*

A total of 33,933 video frames were recorded at 1000 frames for a sample period of 33.9 s. ICV was applied with an interrogation window of 175 × 175 pixels and a subregion template of 125 × 125 pixels. The center of the interrogation region was moved in steps of 50 pixels. The mean velocity at the jet centerline was 2.55 m/s.

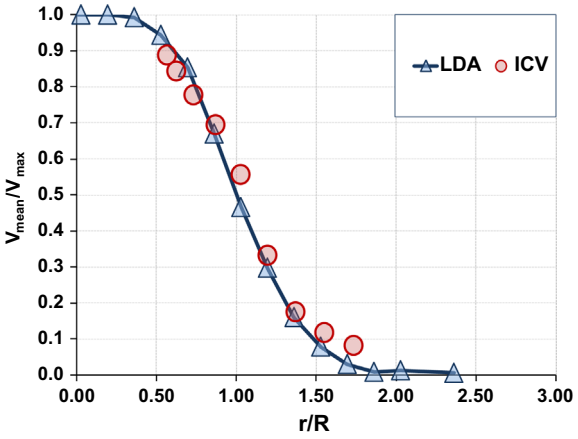

Fig. 27. Radial profiles of streamwise mean velocity at $x/D=2$; 4 in oriice jet; 175 GPM.

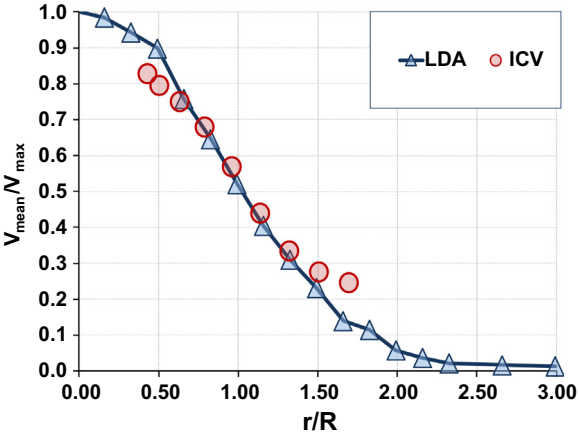

Fig. 28. Radial profiles of streamwise mean velocity at $x/D=4$; 4 in orifice jet; 75 GPM.

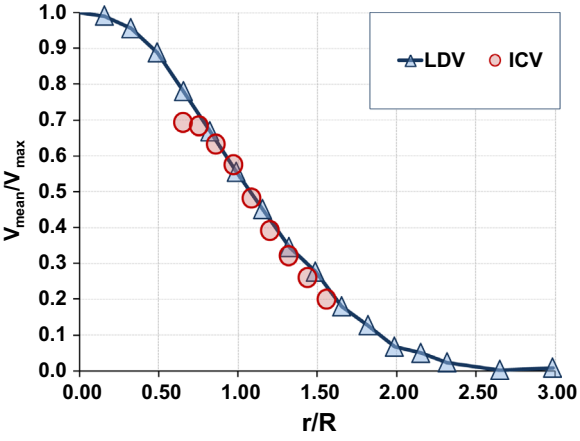

Fig. 29. Radial profiles of streamwise mean velocity at $x/D=2$; 4 in orifice jet; 285 GPM.

3.2.3. Pipe jet at 375 GPM (Re=280,000)

For this case, 34.3 s of high speed video were recorded with dye point injection. A total of 31,265 video frames were recorded (19,100 frames at 1000 frames/s and 12,165 frames at 800 frps) for a total sample period of 34.3 s. ICV was applied with an interrogation window of 175 × 175 pixels and a subregion template of 125 × 125 pixels. The center of the interrogation region was moved in steps of 50 pixels. The mean velocity at the jet centerline was 3.27 m/s.

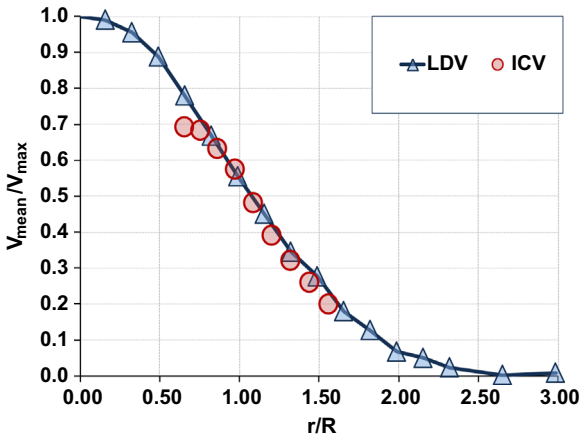

Fig. 30. Radial profiles of streamwise mean velocity at $x/D=4$; 4 in orifice jet; 285 GPM.

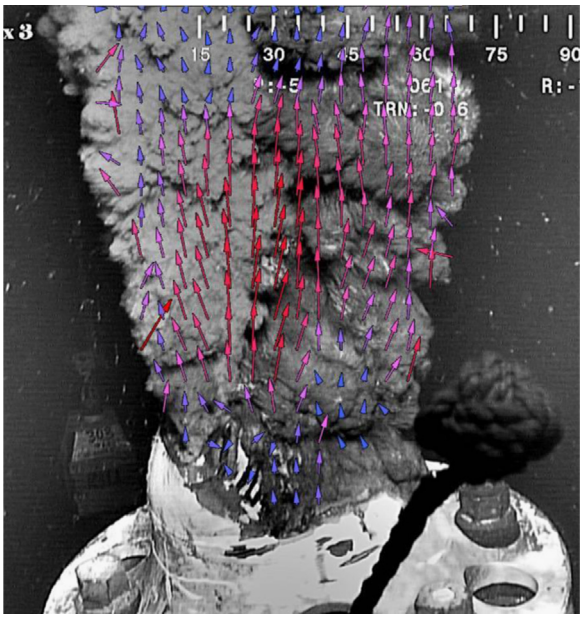

Fig. 31. Overlay of velocity vectors measured with ICV onto one video frame of the DWH oil leak jet taken on June 3, 2010. Pseudocoloring of velocity vectors ranges from blue at 0.1 m/s to red at 0.7 m/s. (For interpretation of the references to color in this figure legend, the reader is referred to the web version of this article.)

3.2.4. Pipe jet at 500 GPM (Re=379,000)

A total of 44,867 video frames were recorded for this case at 1150 frames/s for a total sample period of 39.0 s. To account for larger displacements at this higher jet velocity, ICV was applied with a larger interrogation window of 200 × 200 pixels and a subregion template of 125 × 125 pixels. The center of the interrogation region was moved in steps of 50 pixels. The mean velocity at the jet centerline was 4.31 m/s.

3.2.5. Pipe jet at 660 GPM (Re=500,000)

A total of 44,867 video frames were recorded for this case at 1150 frames/s for a total sample period of 39.0 s. To account for larger displacements at this higher jet velocity, ICV was applied with a larger interrogation window of 200 × 200 pixels and a subregion template of 125 × 125 pixels. The center of the interrogation region was moved in steps of 50 pixels. The mean velocity at the jet centerline was 4.31 m/s.

3.2.6. Orifice jet at 75 GPM (Re=57,000)

For this case, 45.4 s of high speed video of the dye injection stream were recorded: 22,700 video frames were recorded at 500 frames/s. The exposure time was 750 μs. ICV was applied with an interrogation window of 200 × 200 pixels and a subregion template of 100 × 100 pixels. A velocity vector was calculated at increments of 75 pixels. The mean velocity at the jet centerline was 0.74 m/s. The figures below shows the ICV and LDA measurements of mean velocity.

3.2.7. Orifice at 175 GPM (Re=133,000)

For this case, 23.6 s of high speed video of the dye injection stream were recorded: 11,800 video frames at 500 frames/s. The exposure time was 750 μs. ICV was applied with an interrogation window of 150 × 150 pixels and a subregion template of 90 × 90 pixels. A velocity vector was calculated at increments of 50 pixels. The mean velocity at the jet centerline was 1.72 m/s.

3.2.8. Orifice jet at 285 GPM (Re=216,000)

For this case, 43.8 s of high speed video of the dye injection stream were recorded: 21,900 video frames at 500 frames/s. The exposure time was 750 μs. ICV was applied with an interrogation window of 150 × 150 pixels and a subregion template of 90 × 90 pixels. A velocity vector was calculated at increments of 75 pixels. The mean velocity at the jet centerline was 2.62 m/s.

3.3. ICV applied to ROV video of the Deepwater Horizon leak jet

The ICV template matching tool of [29,30] was applied to a 10-s video clip of the Deepwater Horizon leak jet. Fig. 31 shows one frame of the video with velocity vectors measured with PIV software overlain. The video clip was recorded on June 3, 2010, after the riser pipe had been severed just about the Blow Off Preventor. The frame rate was 25 frames per second and the resolution of the field-of-view shown in Fig. 31 is 815 × 890 pixels. An interrogation region of 200 pixels and a template region of 100 pixels was applied at increments of 50 pixels. The radial profile of mean streamwise velocity at $x/D=1$ is shown in Fig. 32.

The direction of the velocity vectors in Fig. 31 appears to be qualitatively correct for most of the jet. The mean velocity measured at $x=1D$ was 0.44 m/s and the mean velocity for the entire jet was 0.35 m/s.

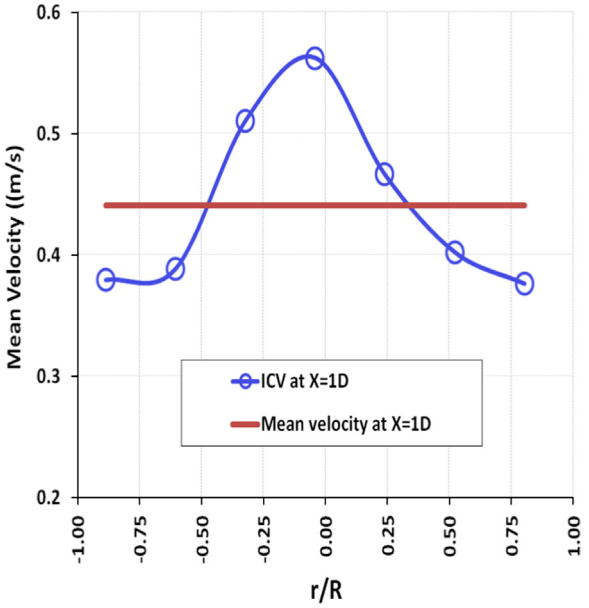

Fig. 32. Radial profile of mean streamwise velocity at $x=1D$ measured with ICV applied to ROV video taken on June 3, 2010.

4. Discussion

Given that our measurements of the dye-colored water jet using PIV software are in good agreement with the LDA measurements, it can be assumed that PIV is a relatively accurate tool for the experimental conditions of the dye-colored jet. The measurements of the DWH oil leak jet by three members of the Plume Team, each using a different PIV software and ROV video taken on June 3, 2010, produced consistent results of mean velocities in the range of 0.4–0.6 m/s. The measurements of this study of the DWH oil leak jet using ICV produced mean velocities of 0.44 m/s, which is in agreement with the results from the Plume Team. However, the velocities produced by manual feature tracking velocimetry (manual FTV) for the same ROV video were much higher, in the range of 1.1–1.5 m/s, and resulted in accurate estimates of the DWH oil leak rate. The leak rate was calculated by the Plume Team with Eq. (4).

Table 1 shows the calculations of the oil leak rate by members of the Plume Team. For the post riser-cut ROV video of June 3, 2010, all members of the Plume Team made their measurements close to the jet exit in the ZFE. The gas-to-oil ratio, X_{GOR}, was measured to be 0.41 by sampling the oil/gas mixture and taking it to the surface for analysis. All members used the cross-sectional area of the jet exit for their calculations. Entrainment was assumed to be negligible close to the jet exit, so the entrainment factor was 1.0.

The members using ICV (PIV software) made an assumption that the mean velocity of the jet near the jet exit was 1.6 times the velocity of visible features as measured with ICV (PIV software). The rationale for a value of 1.6 was based on two assumptions. First, it was assumed that the velocity of coherent structures at the boundary of the jet in the ZFE is equal to the mean streamwise velocity in the ZFE. The second assumption was stated as "*The level of intermittency in the shear layer, γ, is used as a fiduciary indicator of the presence of turbulent coherent structures, so that the average of the mean streamwise velocity weighted with γ provides an estimate of the convection velocity of the jet turbulent structures, which yields a ratio of 1/0.62 ≈ 1.6 between the velocity of the jet coherent structures measured by PIV and the bulk flow velocity at the potential cone of the jet*" [10].

The members using manual FTV also assumed that the velocity of coherent structures at the boundary of the jet in the ZFE is equal to the mean streamwise velocity in the ZFE. However, with manual FTV, only coherent structures were selected and measured, therefore assumptions about the intermittency of coherent structures or the effect of non-coherent structures were not necessary. The resulting estimates of oil leak rate with manual FTV were 38–84% higher than the estimates with PIV.

Table 1
Estimates of oil discharge rate from Deepwater Horizon by members of the FRTG Plume Team.

	Technique	u_{vf}	Intermittency factor	A_{jet}(m^2)	χ_{GOR}	$E(x)$	$\dot{Q}_{oil}$ (barrels/day)
Member A	ICV with PIV software	0.49	1.6	0.19	0.4	1	34,000
Member B	ICV with PIV software	0.50	1.6	0.19	0.4	1	34,000
Member C	ICV with PIV software	0.51	1.6	0.19	0.4	1	35,000
Leifer	Manual FTV	1.4	1.0	0.19	0.4	1	62,500
Savaş	Manual FTV	1.1	1.0	0.19	0.4	1	47,000
Shaffer	Manual FTV	1.4	1.0	0.19	0.4	1	61,000

The Plume Team developed their estimates of the oil leak rate in June and early July of 2010. The oil leak rate was later measured in the final well capping system with an improvised orifice system in late July 2010 and on August 2, 2010, the government announced its official estimate of the oil leak rate to be 53,000 bpd at the time of well capping and 62,000 bpd in April 2010 when the oil leak started [16]. The uncertainty was estimated to be $\pm$10%. The oil leak was also estimated to be in the range of 53,000–62,000 bpd by several other technologies, including sonar measurements, modeling of the well reservoir, and satellite imaging of the oil slick [16].

Since the velocity of the DWH oil leak jet could not be accurately measured with another technique, as the dye-colored jet could be measured with LDA, it is not possible to say how accurate ICV with PIV software was for the DWH oil leak jet. However, the fact that PIV software produced lower velocities that resulted in underestimates of the oil leak rate, suggest that either the PIV software was producing erroneously low velocities, or different assumptions are required for the relationship between the velocity of visible structures and the mean jet velocity.

Crone et al. [6,5] have measured the velocity of visible features on a dye-colored water jet, but at lower Reynolds numbers than in this study. The Reynolds numbers were in the range of 1000–10,000 to simulate hydrothermal ocean vents. They measured velocities of visible features with a custom pixel cross-correlation technique and with PIV software. The pixel correlation technique cross-correlates the gray level signal from two pixels, one downstream of the other. Crone et al. found that velocities measured with PIV software were 50% too low and led to underestimates of the jet flow rate. Crone et al. also applied their cross-correlation technique to ROV video of the DWH oil leak jets and estimated the leak rate to be 56,000 bpd [7].

There are numerous factors that could have influenced the PIV results for the DWH. The frame rate of the ROV cameras was 25 frames/s which was too slow to detect the rapid growth, deformation and decay of smaller scale coherent structures. The frame rate used to record the dye-colored water jet in the Berkeley Tow Tank was in the range of 500–1500 frames/s. This provided good temporal resolution of the smaller coherent structures. Choice of optimal frame rates is being studied in the DOI-BSEE project [9].

Use of PIV software also requires an estimate of the intermittency of coherent structures. Members of the FRTG Plume Team using PIV software estimated the intermittency to be 62%, i.e., coherent structures were present 62% of the time. However, it has not been verified that PIV software is indeed measuring coherent structures 62% of the time.

In this study it was found that PIV results are sensitive to the choice of the sizes of the interrogation and template regions. Using region sizes that are too small tends to produce erroneously low values of velocity near the center of the dye-colored jet. Because of the computation time required for a PIV analysis of high resolution, high speed video, a systematic study of the effect of the sizes of interrogation and template regions was not completed. For each flow condition, 20–50 GBytes of video were analyzed with PIV software. This required 1–2 days of CPU time on an HP Z800 computer with two Intel Xenon liquid cooled CPU's with 6 cores at a clock speed of 3.46 GHz, 96 GBytes of RAM, and a RAID0 array of eight 300 GByte SSD drives. With nine flow conditions, a systematic study of the size of the interrogation region and the template region, using just five size increments for each region, would require 225–450 days of CPU time.

Yet another factor influencing PIV results are the image processing steps used to enhance video images prior to PIV. In this study, a high pass FFT was applied to remove variations in brightness caused by variations in illumination. The high pass FFT was set about 1/4th the width of the field-of-view. Several contrast enhancement steps were applied to enhance the brightness of the dyed features and reduce the areas without dye to a gray level of zero. A median filter with a kernel size of 3×3 was applied to reduce high frequency pixel-to-pixel noise. A Sobel edge detection filter as applied to some of the high speed video prior to PIV software, however, a systematic study was not done, so conclusions cannot be drawn at this time regarding whether or not edge detection improves PIV software results.

5. Conclusions

Application of PIV software to the high speed video of dye-colored jets in the Berkeley Tow Tank produces velocities that are in good agreement with velocities measured with LDA. Application of PIV software to the DWH oil leak jets by several different members of the Plume Team and in this study produced consistent velocities in the range of 0.4–0.6 m/s using ROV video from June 3, 2010 applied close to the jet exit ($x/D < 2$). However, the velocities from PIV software are 2–3 times lower than velocities measured with manual feature tracking by hand. The fact that the estimates of the DWH oil leak rate using velocities from manual tracking were in good agreement with the actual leak rate suggests that the velocities from PIV software are erroneously low, or that different assumptions are required for the intermittency of coherent structures and the relationship between the velocity measured with PIV software and the mean velocity. The studies by Crone et al. support this conclusion. Because the DWH oil leak jet was not well controlled and velocities were not measured with an alternative technique, it is not possible at this time to definitively know why PIV software produced lower velocities. It is recommended that studies be conducted with a well characterized, submerged oil jet. The submerged oil jet should be recorded at very high frame rates to resolve the deformation of smaller scale features. It is also suggested that a systematic study of effect of sizes of interrogation regions be conducted.

References

[1] Abramovich GN. The theory of turbulent jets. MIT Press; 2003.
[2] Albertson ML, Dai YeB, Jensen RA, Rouse H. Diffusion of submerged jets. Trans ASCE 1950;115:629–44.
[3] Bradbury LJS. The structure of a self-preserving turbulent plane jet. J Fluid Mech 1965;23:31–64.
[4] Chen CJ, Rodi W. Vertical turbulent buoyant jets: a review of experimental data. Science and applications of heat and mass transfer, vol. 4. Pergamon Press; 1980.
[5] Crone TJ, Wilcock WSD, McDuff REF. Flow rate perturbations in a black smoker hydrothermal vent in response to a mid-ocean ridge earthquake swarm. Geochemistry Geophysics Geosystems 23 March 2010;11(3):1–3.
[6] Crone TJ, McDuff RE, Wilcock WSD. Optical plume velocimetry: a new flow measurement technique for use in seafloor hydrothermal systems. Experiments in Fluids, Volume 45, Issue 5, p.899-915.
[7] Crone TJ, Tolstoy M. Magnitude of the 2010 Gulf of Mexico oil leak. Science 2010;330(6004):634.
[8] Dantec. 2013. ⟨www.dantecdynamics.com⟩.
[9] DOI-BSEE Project E13PS00032. Development of a ROV deployed video analysis tool for rapid measurement of submerged oil/gas leaks. Department of the Interior, Bureau of Safety and Environmental Enforcement funded project with NETL and UC Berkeley; 2013.
[10] FRTG Plume Analysis Team. Deepwater Horizon Release Estimate of Rate by PIV, ⟨www.doi.gov/deepwaterhorizon⟩; 2010.
[11] Eggers J, Villermaux E. Physics of liquid jets. Reports on Progress in Physics 2008;71:1–79.
[12] Guo B, Langrish TAG, Flecther DF. An Assessment of Turbulence Models applied to the Simulation of a Two Dimensional Submerged Jet. Applied Mathematical Modeling 2001;25(8):635–53.
[13] Lee and Chu, 2003, "Turbulent Jets and Plumes: A Lagrangian Approach," Authors. Joseph Hun-wei Lee and Vincent Chu, Kluwe Academic Publishers ISBN numbers are ISBN-13: 978-1402075209 ISBN-10: 159693350X.
[14] Nikuradse, J. Gesetzmasigkeiten der turbulenten Stromung in glaten Rohren. Translated as 'Laws of turbulent flow in smooth pipes'. NASA TT F-10 359 (1966); 1932.
[15] Nikuradse, J. Stromungsgesetze in rauhen Rohren VDI-Forschungsheft no. 356. Translated as 'Laws of Flow in Rough Pipes',NACA-TM 1292 (1950); 1933.

[16] McNutt MK, Camilli R, Crone TJ, Guthrie GD, Hsieh PA, Ryerson TB, Savaş Ö, Shaffer F. Review of flow rate estimates of the Deepwater Horizon oil spill. (Published online on December 20, 2011). Proc Natl Acad Sci USA 2011. http://dx.doi.org/10.1073/pnas.1112139108.
[17] Miller D, Coming E. Static pressure distribution in the free turbulent jet. J Fluid Mech 1957;3:1–16.
[18] National Commission on the Deepwater Horizon Oil Spill and Offshore Drilling, December 2010. Deepwater: The Gulf Disaster and the Future of Offshore Drilling. Report to the President, available at: www.oilspillcommission.gov.
[19] Papanicolaou P, List EJ. Investigations of round vertical turbulent buoyant jets. J Fluid Mech 1988;209:151–90.
[20] Pope SB. Turbulent flows. Cambridge University Press; 2000 (ISBN: 9780521598866).
[21] Prandtl L. Bericht über Untersuchungen zu ausgebildeten Turbulenz. ZAMM 1925;5:136.
[22] Rajaratnam N. Turbulent jets; developments in water science. Elsevier; 1976 (ISBN 0444413723, 9780444413727).
[23] Savaş Ö. A visual study in the near field of turbulent jets and implications for estimating accidental discharges. (Published online on September 4, 2012). Exp Fluids 2012;53(5):1501–14. http://dx.doi.org/10.1007/s00348-012-1372-7.
[24] Schlichting H, Gersten K. Boundary layer theory. 8th ed. Springer-Verlag; 2004 ISBN:81-8128-121-7.
[25] Schlumberger Report. Fluid analysis on Macondo samples, BP field, Mississippi Canyon 252, well: OCS-G, 32306#1, reservoir sample analysis report. Schlumberger Report 201000053; 2010.
[26] Schneider CA, Rasband WS, Eliceiri KW. NIH Image to ImageJ: 25 years of image analysis. Nat Methods 2012;9:671–5.
[27] Trujillo MF, Hsiao CT, Choi JK, Paterson EG, Chahine GL, Peltier LJ. Numerical and experimental study of a horizontal jet below a free surface. In: Proceedings of the 9th international conference on numerical ship hydrodynamics, Ann Arbor, MI; 2007.
[28] Tseng Q, et al. Spatial organization of the extracellular matrix regulates cell–cell junction positioning. Proc Natl. Acad Sci 2000(2012):. http://dx.doi.org/10.1073/pnas.1106377109.
[29] Tseng Qingzong. Study of multicellular architecture with controlled microenvironment. (Ph.D. dissertation). Université de Grenoble; 2011.
[30] Tseng Q. Template matching and slice alignment—ImageJ plugins 2013.
[31] Wygnanski IJ, Fiedler H. Some measurement in the self-preserving jet. J Fluid Mech 1969;38(3):577–612.